Semi-analytical solutions for solute transport and exchange in fractured porous media

Delphine Roubinet,[1] J.-R. de Dreuzy,[2] and Daniel M. Tartakovsky[1]

Received 19 July 2011; revised 9 November 2011; accepted 15 December 2011; published 27 January 2012.

[1] Fracture-matrix interactions can significantly affect solute transport in fractured porous media and rocks, even when fractures are major (or sole) conduits of flow. We develop a semi-analytical solution for transport of conservative solutes in a single fracture. Our solution accounts for two-dimensional dispersion in the fracture, two-dimensional diffusion in the ambient matrix, and fully coupled fracture-matrix exchange, without resorting to simplifying assumptions regarding any of these transport mechanisms. It also enables one to deal with arbitrary initial and boundary conditions, as well as with distributed and point sources. We investigate the impact of transverse dispersion in a fracture and longitudinal diffusion in the ambient matrix on the fracture-matrix exchange, both of which are neglected in standard models of transport in fractured media.

Citation: Roubinet, D., J.-R. de Dreuzy, and D. M. Tartakovsky (2012), Semi-analytical solutions for solute transport and exchange in fractured porous media, *Water Resour. Res.*, *48*, W01542, doi:10.1029/2011WR011168.

1. Introduction

[2] Fracture-matrix interactions can significantly affect solute transport in fractured porous media and rocks, even when fractures are major (or sole) conduits of flow. *Bodin et al.* [2003] provided a thorough review of experimental and theoretical studies that identified advection, dispersion, channeling effects, matrix diffusion, and sorption reactions as key fracture-scale transport mechanisms. Our analysis focuses on the relative effects of advective-dispersive transport in a fracture and molecular diffusion in the ambient matrix.

[3] The first analytical treatment of these combined transport mechanisms is generally attributed to *Tang et al.* [1981], who considered transport in a single fracture imbedded in a semi-infinite matrix. Their solution was extended by *Sudicky and Frind* [1982] to account for the presence of neighboring parallel fractures. These analytical solutions are routinely used to interpret field and experimental observations [*Callahan et al.*, 2000; *Maloszewski and Zuber*, 1993; *Moreno et al.*, 1985; *Zhou et al.*, 2007] and to simulate transport in fractured media with complex fracture geometries [*Liu et al.*, 2007; *Roubinet et al.*, 2010].

[4] Given the widespread use of the *Tang et al.* [1981] and *Sudicky and Frind* [1982] analytical solutions, it is important to ascertain their limitations. Both solutions assume that transport in a fracture is one-dimensional and advection-dominated, i.e., they neglect the transverse variability of solute concentration in the fracture. They also assume matrix diffusion to be one-dimensional, in the direction perpendicular to the fracture, i.e., they neglect the longitudinal variability of solute concentration in the matrix. A final assumption is to replace the full coupling of transport processes in the fracture and the ambient matrix with a one-way coupling, which represents the fracture-matrix exchange (expressed in terms of matrix properties) via a source term in the fracture transport equation. This partial coupling implies that the fracture-matrix exchange is driven by matrix properties and that solute is perfectly mixed throughout the fracture aperture regardless of its width and transport conditions. These assumptions are not universally valid, being appropriate for some parameter values and/or initial and boundary conditions but not for others.

[5] For example, the experiments conducted on centimeter-to-decimeter cores of fractured volcanic tuff [*Callahan et al.*, 2000] found the ratio of fracture to matrix diffusion and the fracture Péclet number to be large enough to justify the assumptions of the *Tang et al.* [1981] and *Sudicky and Frind* [1982] solutions. On the other hand, the field-scale data reviewed by *Zhou et al.* [2007] suggest that equivalent matrix diffusion increases with the observation scale, reaching values that may undermine the validity of the assumptions underlying the solutions of *Tang et al.* [1981] and *Sudicky and Frind* [1982]. (It is worthwhile emphasizing that these and other experimental studies do not measure matrix diffusion directly, inferring it instead from analytical or numerical solutions of the transport equations.) The numerical simulations of *Buckley and Loyalka* [1994] revealed that solute concentration is sensitive to parameters that are absent in these solutions, further undermining their universality.

[6] The main goal of our analysis is to provide a closed-form, computationally efficient description of transport of solutes in a fracture and their exchange with the ambient matrix. We derive a semi-analytical solution for transport in a fracture imbedded in the semi-infinite matrix, without resorting to the simplifying assumptions of *Tang et al.* [1981] and *Sudicky and Frind* [1982]. Our solution accounts for transverse dispersion in the fracture, two-dimensional diffusion in the matrix, and matrix anisotropy

[1]Department of Mechanical and Aerospace Engineering, University of California, San Diego, La Jolla, California, USA.
[2]Géosciences Rennes, UMR CNRS 6118, Université de Rennes I, Rennes, France.

0043-1397/12/2011WR011168

(with differing transverse and longitudinal diffusion coefficients in the matrix). It reduces to the solution of *Tang et al.* [1981] in the limit of the longitudinal diffusion coefficient in the matrix going to zero and the transverse dispersion in the fracture going to infinity. Finally, unlike its existing counterparts, our solution is capable of handling both point and distributed sources whose strength may vary in space and/or time.

[7] We used our solution to determine the limits of applicability of the *Tang et al.* [1981] analysis and to investigate the relative impact of various transport parameters, in both the fracture and the ambient matrix, on solute migration through fractured rocks. Other uses of our solution include the validation of numerical codes and its deployment as a component in systems-based models of complex subsurface systems. In the latter application, the matrix represents a low-permeability portion of a flow domain (e.g., mildly fractured "safe" rock) and the diffusion coefficients represent effective transport properties. The rock's heterogeneity and the topology of its fracture network might result in two-dimensional anisotropic effective diffusion that can be modeled with our solution.

[8] The solution developed in this study describes a general transport phenomena occurring in mobile-immobile environments. Transport in aquifer-aquitard systems is another example of such processes, which has been studied analytically by *Zhan et al.* [2009]. Their study focused on the relative effects of the transport parameters controlling the transverse solute spreading (transverse dispersion in an aquifer and transverse advection in an aquitard) and did not consider longitudinal diffusion in the immobile part. Despite certain similarities between the two solutions, our solution is different in both its methodology and its scope. The former difference stems from the fact that our solution is based on the Green's functions, which provide it with a solid mathematical foundation and allow for the presence of nontrivial initial and boundary conditions, sources, and sinks. As far as the scope is concerned, we will demonstrate that the *Zhan et al.* [2009] conclusions are specific to systems that exhibit a strong transverse displacement in the aquitard and are not applicable to classical fracture-matrix systems.

[9] A mathematical formulation of the transport problem is presented in section 2. Section 3 contains the semi-analytical solution in the form of a Fredholm equation. This solution is used in section 4 to explore the impact of transport parameters on fracture-matrix exchange and to identify a parameter range within which a two-dimensional solution reduces to a one-dimensional solution, as the solution of *Tang et al.* [1981]. Conclusions and implications of our study are summarized in section 5.

2. Problem Formulation

[10] Consider transport of a conservative solute in a single fracture with half-aperture b, embedded in an infinite matrix (Figure 1). The solute concentration $c_f(x,z,t)$ in the fracture $\Omega_f = \{(x,z) : 0 \le x < \infty, 0 \le z \le b\}$ satisfies an advection-dispersion equation

$$\frac{\partial c_f}{\partial t} + u\frac{\partial c_f}{\partial x} = D_L^f \frac{\partial^2 c_f}{\partial x^2} + D_T^f \frac{\partial^2 c_f}{\partial z^2} + f, \quad (x,z) \in \Omega_f, \qquad (1)$$

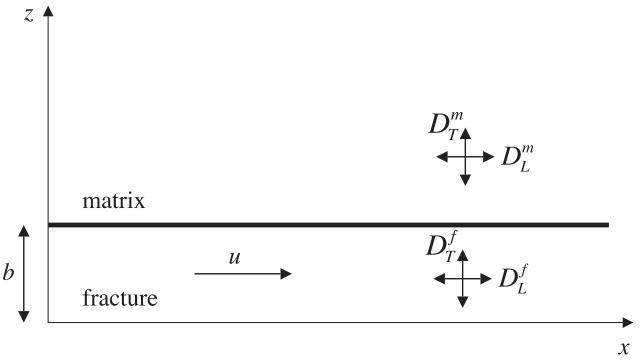

Figure 1. A schematic representation of the fracture-matrix system.

where u is the (constant) macroscopic fluid velocity, $f(x,z,t)$ is a source term, and $D_L^f = D_m + \alpha_L u$ and $D_T^f = D_m + \alpha_T u$ are the longitudinal and transverse dispersion coefficients, respectively. Here D_m is the molecular diffusion coefficient, and α_L and α_T are the longitudinal and transverse dispersivities, respectively.

[11] The ambient matrix $\Omega_m = \{(x,z) : 0 \le x < \infty, b \le z < \infty\}$ is assumed to be impervious to flow. The solute spreads throughout the matrix by diffusion. Its concentration in the matrix $c_m(x,z,t)$, is governed by a diffusion equation

$$\frac{\partial c_m}{\partial t} = D_L^m \frac{\partial^2 c_m}{\partial x^2} + D_T^m \frac{\partial^2 c_m}{\partial z^2}, \quad (x,z) \in \Omega_m, \qquad (2)$$

where D_L^m and D_T^m are the longitudinal and transverse diffusion coefficients, respectively. While hydrogeologists typically treat effective molecular diffusion in porous media as isotropic, numerous theoretical (e.g., *Battiato et al.* [2009], *Battiato and Tartakovsky* [2011], and references therein) and experimental (e.g., *Van Loon et al.* [2004], *Altmann et al.* [2012], and references therein) studies demonstrate that it can be anisotropic. The formulation (2) with $D_L^m \ne D_T^m$ allows for this eventuality.

[12] Let $c_f^0(x,z)$ and $c_m^0(x,z)$ denote the solute's concentrations, at time $t = 0$, in the fracture and the matrix, respectively. Then the transport equations (1) and (2) are subject to initial conditions

$$c_f(x,z,0) = c_f^0(x,z), \quad c_m(x,z,0) = c_m^0(x,z). \qquad (3a)$$

At the fracture-matrix interface $z = b$, both the solute concentration and the mass flux are continuous, giving rise to two interfacial conditions

$$c_f = c_m, \quad D_T^f \frac{\partial c_f}{\partial z} = \phi_m D_T^m \frac{\partial c_m}{\partial z} \equiv r, \quad z = b, \qquad (3b)$$

where ϕ_m is the matrix porosity, and $r(x,t)$ is the (unknown) mass flux between the fracture and the ambient matrix. Equation (1) is also subject to boundary conditions

$$c_f(0,z,t) = c_0, \qquad c_f(\infty,z,t) = 0, \qquad \frac{\partial c_f}{\partial z}(x,0,t) = 0, \qquad (3c)$$

where $c_0(z,t)$ is the prescribed concentration at the fracture's inlet, and the latter condition reflects the concentration's symmetry with respect to the fracture's center $z = 0$. Finally, equation (2) is subject to boundary conditions

$$c_m(0,z,t) = 0, \qquad c_m(\infty,z,t) = 0, \qquad c_m(x,\infty,t) = 0. \quad (3d)$$

Equations (1), (2) and (3a)–(3d) represent a coupled system of two boundary-value problems (BVPs). They are solved below by means of the Green's functions.

3. Solution Formulation

3.1. General Solution

[13] Let $G^f(x,z;x',z';t-t')$ denote the Green's function for the fracture BVP (1), (3a), (3c), and $D_T^f \partial c_f/\partial z\,(x,z=b,t) = r$, and $G^m(x,z;x',z';t-t')$ the Green's function for the matrix BVP (2), (3a), (3d), and $\phi_m D_T^m \partial c_m/\partial z(x,z=b,t) = r$. Their analytical expressions are given in Appendix A.

[14] Solutions of the two BVPs, expressed in terms of the corresponding Green's functions, yield the solute concentrations in the fracture (A9) and the matrix (A10). Their Laplace transforms,

$$\overline{\mathcal{A}}(s) = \int_0^\infty \mathcal{A}(t) e^{-st}\,\mathrm{d}t, \qquad \forall \qquad \mathcal{A}(t) \quad (4)$$

take the form

$$\begin{aligned}\overline{c}_f = &\int_0^b\int_0^\infty c_f^0 \overline{G}^f\,\mathrm{d}x'\mathrm{d}z' + \int_0^b \overline{c}_0 \left[u\overline{G}^f + D_L^f \frac{\partial \overline{G}^f}{\partial x'}\right]_{|x'=0} \mathrm{d}z' \\ &+ \int_0^\infty \overline{r}\,\overline{G}^f_{|z'=b}\,\mathrm{d}x' + \int_0^b\int_0^\infty \overline{f}\,\overline{G}^f\,\mathrm{d}x'\mathrm{d}z'\end{aligned} \quad (5)$$

and

$$\overline{c}_m = \int_b^\infty\int_0^\infty c_m^0 \overline{G}^m\,\mathrm{d}x'\mathrm{d}z' - \frac{1}{\phi_m}\int_0^\infty \overline{r}\,\overline{G}^m_{|z'=b}\,\mathrm{d}x', \quad (6)$$

where the Laplace transforms $\overline{G}^f$ and $\overline{G}^m$ of the Green's functions G^f and G^m are given by (A3)–(A5) and (A8), respectively.

[15] The Laplace transform of the fracture-matrix exchange rate, $\overline{r}(x,s)$, is obtained from the first continuity condition in (3b) which yields

$$\overline{c}_f(x,z=b,s) = \overline{c}_m(x,z=b,s). \quad (7)$$

Combining (5)–(7) yields a Fredholm equation of the first kind for $\overline{r}(x,s)$. A numerical algorithm used to solve this equation is described in Appendix B.

3.2. Explicit Semi-analytical Expression

[16] To demonstrate the salient features of our solution and to explore its parameter space, we consider solute transport with zero initial concentrations in the fracture and the ambient matrix, ($c_f^0 = 0$ and $c_m^0 = 0$), in the absence of internal sources/sinks ($f = 0$), driven by the uniform concentration at the fracture's inlet, $c_0(t)$. This corresponds to the transport regime considered by *Tang et al.* [1981].

[17] With these driving forces, (5) and (6) reduce to

$$\overline{c}_f = \overline{c}_0 \int_0^b \left[u\overline{G}^f + D_L^f \frac{\partial \overline{G}^f}{\partial x'}\right]_{|x'=0} \mathrm{d}z' + \int_0^\infty \overline{r}\,\overline{G}^f_{|z'=b}\,\mathrm{d}x' \quad (8)$$

and

$$\overline{c}_m = -\frac{1}{\phi_m}\int_0^\infty \overline{r}\,\overline{G}^m_{|z'=b}\,\mathrm{d}x'. \quad (9)$$

Let us introduce dimensionless parameters

$$Pe = \frac{ub}{\sqrt{D_L^f D_T^f}}, \qquad D_{fm} = \frac{\sqrt{D_L^f D_T^f}}{\phi_m \sqrt{D_L^m D_T^m}}, \quad (10)$$

dimensionless independent variables

$$\begin{aligned} s_f &= \frac{b^2 s}{D_T^f}, \qquad s_m = \frac{b^2 s}{D_T^m}, \qquad z_m = \frac{z}{b}, \\ x_f &= \frac{x}{b}\sqrt{\frac{D_T^f}{D_L^f}}, \qquad x_m = \frac{x}{b}\sqrt{\frac{D_T^m}{D_L^m}}, \end{aligned} \quad (11)$$

and normalized dependent variables

$$\overline{C}_f = \frac{\overline{c}_f}{\overline{c}_0}, \qquad \overline{C}_m = \frac{\overline{c}_m}{\overline{c}_0}, \qquad \overline{R} = \frac{\overline{r}}{\overline{c}_0}. \quad (12)$$

Substituting (A3)–(A5) and (A8) into (8) and (9) leads to

$$\begin{aligned}\overline{C}_f = F_1^*(x_f) + \frac{1}{\sqrt{D_L^f D_T^f}}\int_0^\infty \overline{R}\Big[&\frac{1}{2}F_2^*(x_f,x_f',s_f) \\ &+ \sum_{n=1}^{+\infty}(-1)^n \cos(n\pi z_m) F_2^*(x_f,x_f',s_f+n^2\pi^2)\Big]\mathrm{d}x'\end{aligned} \quad (13)$$

and

$$\overline{C}_m = \frac{1}{\pi\phi_m\sqrt{D_L^m D_T^m}}\int_0^\infty \overline{R}\,F_3^*(x_m,x_m',z_m,s_m)\mathrm{d}x'. \quad (14)$$

Here the functions $F_1^*(x,s)$, $F_2^*(x,x',s)$, and $F_3^*(x,x',z,s)$ are given by

$$F_1^* = f_1^*(x) f_2^*(x,s), \quad (15a)$$

$$F_2^* = f_1^*(x-x')\frac{f_2^*(|x-x'|,s) - f_2^*(x+x',s)}{\sqrt{Pe^2/4+s}}, \quad (15b)$$

$$F_3^* = K_0(\sqrt{\beta_1 s}) - K_0(\sqrt{\beta_2 s}), \tag{15c}$$

with

$$f_1^*(x) = e^{xPe/2}, \qquad f_2^*(x,s) = e^{-x\sqrt{Pe^2/4+s}}, \tag{15d}$$

$\beta_1 = (x_m + x_m')^2 + (z_m - 1)^2$, $\beta_2 = (x_m - x_m')^2 + (z_m - 1)^2$, and $K_0(\cdot)$ denoting the modified Bessel function.

[18] Equating (13) with (14), both evaluated at $z_m = 1$, yields a Fredholm equation for $\overline{R}(x,s)$,

$$\int_0^\infty \mathcal{K}(x,x',s)\overline{R}(x',s)\mathrm{d}x' = -\sqrt{D_L^f D_T^f}F_1^*(x_f,s), \tag{16}$$

where the kernel $\mathcal{K}(x,x',s)$ has the form

$$\mathcal{K} = \frac{1}{2}F_2^*(x_f,x_f',s_f) + \sum_{n=1}^{+\infty}F_2^*(x_f,x_f',s_f+n^2\pi^2) - D_{fm}F_3^*(x_m,x_m',z_m=1,s_m). \tag{17}$$

This integral equation is solved numerically following the procedure outlined in Appendix B.

4. Results

[19] Unless specified otherwise, the results reported below represent the relative fracture concentration $C_f = c_f/c_0$ averaged over the aperture width. We call the concentration $C_f(x,t)$ computed with the full model, which accounts for both transverse dispersion in the fracture (D_T^f) and longitudinal diffusion in the matrix (D_L^m) and fully couples transport in the fracture and matrix domains, a "2-D solution." The limit of this solution as $D_T^f \to \infty$ (complete instantaneous mixing throughout the fracture's aperture) and $D_L^m \to 0$ (no longitudinal diffusion in the matrix) is referred to as a "1-D solution." (Computationally, the limits $D_T^f \to \infty$ and $D_L^m \to 0$ indicate the use of a sufficiently large value of D_T^f and a sufficiently small value of D_L^m, such that their respective increase and decrease do not affect the simulation results.) The 1-D solution preserves the full fracture-matrix coupling. This is in contrast to the *Tang et al.* [1981] solution, which relies on the partial fracture-matrix coupling and corresponds to $D_T^f \to \infty$ and $D_L^m = 0$. Table 1 contains default (reference) parameter values similar to those used by *Tang et al.* [1981]. The Stehfest algorithm with 12 terms was used to compute the Laplace transforms.

4.1. Comparison with the *Tang et al.* [1981] Solution

[20] Figure 2 exhibits the fracture concentration profiles $C_f(x,t)$ computed alternatively with the 1-D and *Tang et al.* [1981] solutions at $t = 10^5$, 10^6, and 10^7 s. The parameters are set to their "high-velocity" default values in Table 1, except for $D_T^f \to \infty$ and $D_L^m = 0$. The two solutions yield identical concentration profiles $C_f(x,t)$, demonstrating that in this transport regime the one-way coupling of *Tang et al.* [1981] might be appropriate.

Table 1. The Default Parameter Values

Parameter	Symbol	Low-Velocity	High-Velocity
Fracture flow velocity	u	10^{-7} m s^{-1}	10^{-5} m s^{-1}
Fracture aperture	b	5×10^{-5} m	10^{-4} m
Longitudinal dispersion in fracture	D_L^f	10^{-9} m^2 s^{-1}	10^{-5} m^2 s^{-1}
Transverse dispersion in fracture	D_T^f	10^{-9} m^2 s^{-1}	10^{-7} m^2 s^{-1}
Longitudinal diffusion in matrix	D_L^m	10^{-10} m^2 s^{-1}	10^{-10} m^2 s^{-1}
Transverse diffusion in matrix	D_T^m	10^{-10} m^2 s^{-1}	10^{-10} m^2 s^{-1}
Matrix porosity	φ_m	0.01	0.35

4.2. Effects of Transverse Dispersion in Fracture

[21] The absence of transverse dispersion in the analytical solutions of *Tang et al.* [1981] and *Sudicky and Frind* [1982] is equivalent to the assumption that the parameter D_T^f is large enough to allow for complete mixing of the solute throughout the fracture aperture. Figure 3 demonstrates the impact of this approximation on predictions of both the average solute concentration in the fracture (Figure 3a) and the cumulative fracture/matrix exchange (Figure 3b). With a few exceptions specified below, e.g., $b = 10^{-3}$ m, the parameters are set to their "high-velocity" default values in Table 1. To isolate the effects of transverse dispersion in the fracture, we set $D_L^m = 0$ and report the results in terms of the ratio $\beta = D_T^f/D_T^m$ of the transverse transport coefficients in the fracture and the matrix.

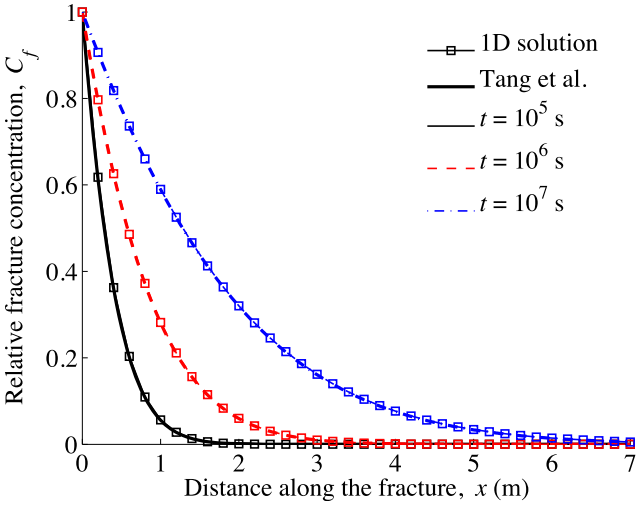

Figure 2. Relative solute concentration in the fracture, $C_f(x,t)$, computed with the 1-D (lines with squares) and *Tang et al.* [1981] (lines) solutions at times $t = 10^5$ s (solid lines), 10^6 s (dashed lines), and 10^7 s (dash-dotted lines). The parameters are set to their "high-velocity" default values (Table 1), except for $D_T^f \to \infty$ and $D_L^m = 0$.

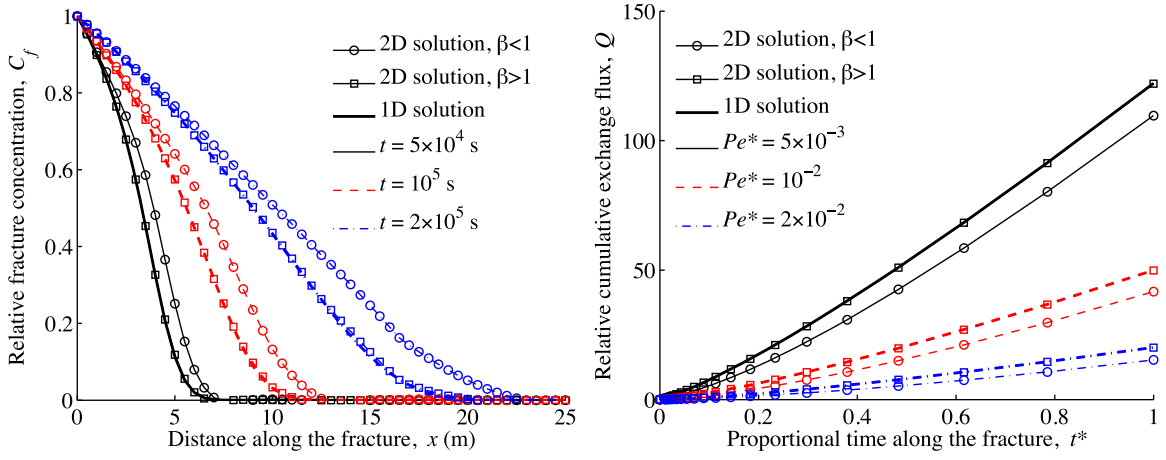

(a) Average relative solute concentration in the fracture (b) Relative cumulative fracture-matrix exchange

Figure 3. l- and 2-D solutions of (a) solute concentration C_f at times $t = 5 \times 10^4$ s (solid lines), $t = 10^5$ s (dashed lines), and $t = 2 \times 10^5$ s (dash-dotted lines), and (b) cumulative exchange rate Q for $Pe^* = 5 \times 10^{-3}$ (solid lines), 10^{-2} (dashed lines), and 2×10^{-2} (dash-dotted lines). The parameters are set to their "high-velocity" default values (Table 1) except for (Figure 3a) $b = 10^{-3}$ m and $u = 10^{-4}$ m s^{-1} and (Figure 3b) $u = 5 \times 10^{-5}$, 10^{-4}, and 2×10^{-4} m s^{-1}. In the 2-D solution, $D_L^m \to 0$.

[22] Figure 3a shows the concentration profiles $C_f(x)$ computed with the l- and 2-D solutions for $u = 10^{-4}$ m s^{-1}. For $\beta \geq 1$, the two solutions coincide, i.e., transverse dispersion in the fracture has no discernible impact on the concentration profiles. In other words, if D_T^m is small ($D_T^m = 10^{-10}$ m^2 s^{-1} in our simulations), changes in D_T^f do not affect the concentration profiles as long as its value remains larger than D_T^m, i.e., the condition $\beta \geq 1$ holds. In this transport regime, transverse diffusion in the matrix is the limiting parameter that controls both solute transfer from the fracture to the matrix and its concentration in the fracture. For $\beta \leq 1$, the errors introduced by the l-D solution (i.e., by neglecting transverse dispersion in the fracture) become discernible, and they grow with time. The 2-D solution reveals that for a given value of D_T^f ($D_T^f = 10^{-9}$ m^2 s^{-1} in our simulations), changes in D_T^m do not affect the concentration profiles as long as its value remains larger than D_T^f, i.e., the condition $\beta \leq 1$ holds. In this transport regime, which is atypical for transport in classical fracture-matrix systems, transverse dispersion in the fracture is the limiting parameter that reduces the fracture-matrix exchange and, correspondingly, increases the solute concentration in the fracture.

[23] Figure 3b exhibits the temporal evolution of the cumulative relative exchange

$$Q(t^*) = \int_0^{t^* t_a} \int_0^{\infty} \frac{r(x,t)}{uc_0} \mathrm{d}x\mathrm{d}t, \tag{18}$$

where $r(x,t)$ is the mass flux between the fracture and the ambient matrix defined by the second equation in (3b), and computed by solving numerically (16). The temporal fraction $t^* \equiv t/t_a \in [0,1]$ is the time t normalized with the advection time $t_a = x_a/u$ for a given distance x_a. It can be expressed in terms of the Péclet number Pe and the dimensionless coordinate x_f and time $t_f = D_T^f t/b^2$ as

$$t^* = Pe \frac{t_f}{x_f}, \tag{19}$$

where Pe and x_f are defined in (10) and (11), respectively. The mass exchange between the fracture and the matrix is normalized with the total mass flux entering the fracture, uc_0. In the simulations reported in Figure 3b, we set $x_a = 10$ m and consider several values of flow velocity $u = 5 \times 10^{-5}$, 10^{-4}, and 2×10^{-4} m s^{-1}. For the Péclet number defined as $Pe^* = ub/D_L^f$, this corresponds to $Pe^* = 5 \times 10^{-3}$, 10^{-2}, and 2×10^{-2}.

[24] Consistent with the concentration results reported in Figure 3a, the l- and 2-D solutions predict the identical cumulative fracture/matrix exchange $Q(t^*)$ when $\beta > 1$, i.e., when transverse dispersion in the fracture (D_T^f) is larger than transverse diffusion (D_L^m) in the matrix. The l-D solution underestimates the cumulative fracture/matrix exchange $Q(t^*)$ when $\beta < 1$, with the errors growing with time.

[25] These findings are in agreement with those obtained by *Zhan et al.* [2009] for the mass exchange in an aquifer-aquitard system. Specifically, they found that the l-D solution (labeled as the "AA method" by *Zhan et al.* [2009]) overestimates the mass exchange when transverse displacement in the aquitard exceeds that in the aquifer, i.e., when $\beta < 1$ in our notation. It is worthwhile noting that in the work of *Zhan et al.* [2009], this result is

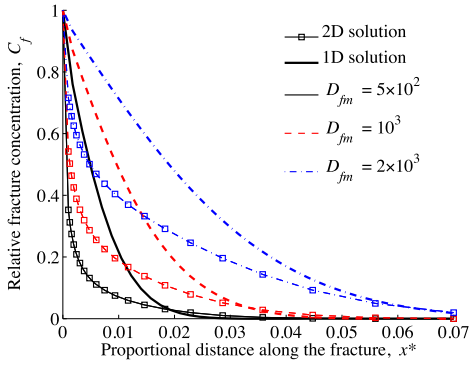

(a) $Pe = 10^{-3}$

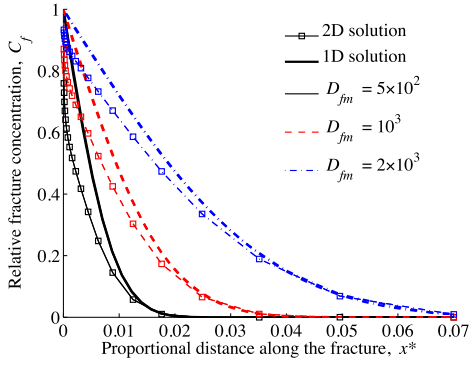

(b) $Pe = 10^{-2}$

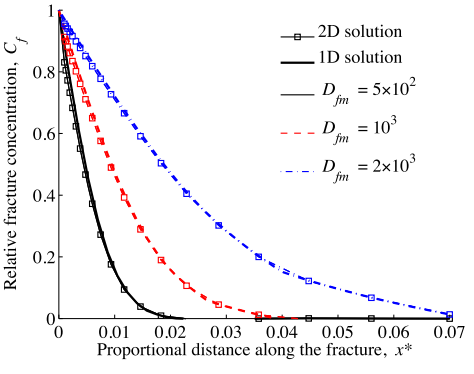

(c) $Pe = 10^{-1}$

Figure 4. Spatial profiles of the relative fracture concentration computed with the 1- (lines) and 2-D (lines with squares) solutions. The parameters are set to their "low-velocity" default values (Table 1), except for ϕ_m and u whose variation results in $D_{fm} = 5 \times 10^2$ (solid lines), 10^3 (dashed lines), and $D_{fm} = 2 \times 10^3$ (dash-dotted lines), and (a) $Pe = 10^{-3}$, (b) 10^{-2}, and (c) $Pe = 10^{-1}$. In the 2-D solution, $D_T^f \to \infty$.

preordained by their formulation of the exchange term, which is defined in terms of the aquitard properties. In our solution, the exchange between mobile and immobile domains is an emerging characteristic determined by the full explicit coupling of transport processes in the two domains.

[26] While not shown here, we found that the relative error between the 1- and 2-D solutions for the fracture-matrix exchange with $\beta < 1$ increases as the Péclet number decreases, i.e., the impact of transverse dispersion in the fracture decreases with Pe. This is because flow velocity (u) and longitudinal dispersion in the fracture (D_L^f), two parameters defining Pe, affect the solute's interfacial concentration. Small u results in slow renewal of the solute at the fracture/matrix interface and large D_L^f leads to longitudinal sprawl, both of which decrease the interfacial concentration. These phenomena enhance the effects of transverse dispersion in the fracture.

[27] This analysis suggests that transverse dispersion might play an important role in aquifer/aquitard systems with $\beta < 1$, which is the case considered by *Zhan et al.* [2009]. Fracture/matrix systems, which are the focus of our analysis, are typically characterized by $\beta > 1$, so that transverse dispersion in the fracture does not impact the fracture/matrix exchange.

4.3. Effects of Longitudinal Diffusion in Matrix

[28] Figure 4 demonstrates the effects of longitudinal diffusion in the matrix (D_L^m) on the solute concentration in the fracture, $C_f(x)$, computed alternatively with the 1- (which is independent of D_L^m) and the 2-D solution (which depends on D_L^m). Except for flow velocity u and matrix porosity ϕ_m, all of the parameters in these simulations are set to their "low-velocity" default values in Table 1. The values of u and ϕ_m vary to yield the following dimensionless parameters in (10): $Pe = 10^{-3}$, 10^{-2}, and 10^{-1}, and $D_{fm} = 5 \times 10^2$, 10^3, and 2×10^3. To isolate the effects of longitudinal diffusion in matrix, we set $D_T^f \to \infty$.

[29] The concentration C_f is plotted as a function of the relative distance along the fracture, $x^* \equiv x/x_a$, where $x_a = ut_a$ is the distance the solute would reach solely due to advection by a certain time t_a (in these simulations we set $t_a = 2.5 \times 10^9$ s). This allows us to compare the impact of longitudinal diffusion on fracture concentration for several values of flow velocities u. In terms of the dimensionless parameters defined above, x^* is given by

$$x^* = \frac{x_f}{Pe\, t_f}. \tag{20}$$

[30] Figure 4 reveals that the magnitude of flow velocity u has no discernible effect on the solute concentration profiles $C_f(x^*)$ computed with the 1-D solution, i.e., when $D_T^f \to \infty$ and $D_L^m \to 0$. It also demonstrates that longitudinal diffusion in the matrix (the 2-D solution corresponding to finite values of D_L^m) decreases the solute concentration $C_f(x^*)$ due to the corresponding increase in the fracture-matrix exchange. It is observed in the transport regimes for which both D_{fm} (the ratio between fracture dispersion and matrix diffusion) and Pe (the Péclet number) are small (Figure 4a).

4.4. Pulse Injection at Fracture Inlet

[31] Since our solution is expressed in terms of the Green's functions, it is capable of handling an arbitrary

juxtaposition of driving forces, such as space-time varying sinks, sources, and initial and boundary conditions. We demonstrate this versatility by considering pulse injection at the fracture inlet ($x = 0$) of solute mass $M = uc_0t_i$ during the injection time interval $0 \leq t \leq t_i$. At $x = 0$, the solute concentration c_0 along the fracture's aperture is uniform and constant during the injection time t_i.

[32] The average normalized concentration in the fracture, $C_f^* \equiv C_f/M$, at the fracture outlet ($x_a = 1$ m) is shown in Figure 5 as a function of the temporal fraction t^* defined by (19). These simulations correspond to the injection interval $t_i = 10$ s. The other parameters are set to their "low-velocity" default values in Table 1. We consider the three flow velocities u corresponding to $Pe = 10^{-3}$, 5×10^{-3}, and 10^{-2}.

[33] Temporal variability of the solute injection magnifies the disparity between the 1- and 2-D solutions, especially for small Péclet numbers ($Pe \leq 10^{-3}$). By accounting for both longitudinal diffusion in the matrix and the dependence of matrix diffusion of transport in the fracture, the 2-D solution predicts that the fracture/matrix exchange occurs closer to the fracture outlet than does the 1-D solution. Consequently, longitudinal diffusion in the matrix reduces both the amplitude and the range of solute arrival times. This effect is amplified by the enhanced storage of solute in the matrix. Similar to the case of constant solute injection, the fracture concentration C_f is affected by transverse diffusion in the matrix (especially when the Péclet number is small) and is largely insensitive to transverse dispersion in the fracture.

[34] The breakthrough curves predicted with the 2-D solution separate the solute dispersing through the fracture from the solute that diffuses the same distance (at later times, of course) through the matrix. Such breakthroughs are precisely what are measured in a tracer experiment, since not all of the solute injected at the fracture's inlet reaches its outlet. By ignoring this effect, the 1-D solution overpredicts the spread of arrival times. Consequently, the reliance on the 1-D solutions (including the *Tang et al.* [1981] solution) to analyze tracer-test data overestimates molecular diffusion.

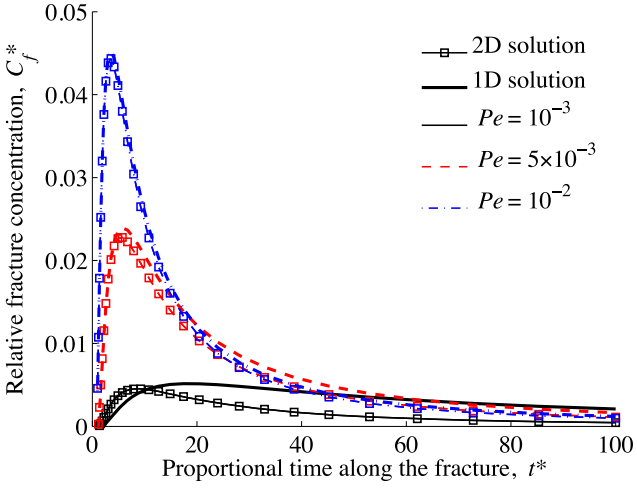

Figure 5. Pulse injection: Temporal evolution of the relative solute concentration in the fracture computed with the 1- (lines) and 2-D (lines with squares) solutions. The parameters are set to their "low-velocity" default values (Table 1), with variations of u leading to $Pe = 10^{-3}$ (solid lines), 5×10^{-3} (dashed lines), and $Pe = 10^{-2}$ (dash-dotted lines).

5. Conclusions

[35] We developed a semi-analytical solution for transport of conservative solutes in a single fracture. Our solution accounts for two-dimensional (2-D) dispersion in the fracture, 2-D diffusion in the ambient matrix, and fully coupled fracture-matrix exchange, without resorting to simplifying assumptions regarding any of these transport mechanisms. It enables one to deal with arbitrary initial and boundary conditions, as well as with distributed and point sources. Consequently, our solution generalizes the widely used solutions of *Tang et al.* [1981] and *Sudicky and Frind* [1982], both of which neglect transverse dispersion in a fracture and longitudinal diffusion in the ambient matrix, and replace the full coupling between the transport processes in the fracture and the matrix with a partial (one-way) coupling.

[36] Our analysis leads to the following major conclusions.

[37] 1. Transverse diffusion in the matrix is the key process controlling the fracture-matrix exchange, if the transverse matrix diffusion coefficient (D_T^m) is smaller than the transverse dispersion coefficient in the fracture (D_T^f).

[38] 2. If $D_T^m > D_T^f$, the fracture-matrix exchange is controlled by transverse dispersion in the fracture, as quantified by the corresponding Péclet number. The assumption of complete mixing in the fracture leads to an overestimation of the fracture-matrix exchange. This effect is enhanced for small Péclet numbers.

[39] 3. Longitudinal diffusion in the matrix has an impact on the fracture concentration for a small Péclet number. Ignoring this process leads to an overestimation of the fracture concentration. This effect becomes more pronounced as the ratio D_T^f/D_T^m decreases.

[40] 4. Longitudinal diffusion in the matrix decreases both the magnitude and range of arrival times in pulse-injection tracer experiments. The standard fracture/matrix transport models ignore this process, leading to the overestimation of the transport parameters from tracer tests. By accounting for longitudinal diffusion in the matrix our solution improves the interpretation of tracer tests in fractured media.

[41] The methodology developed in the present analysis can be extended to account for the spatial fracture-scale variability of flow velocity. Numerical studies [*Buckley and Loyalka*, 1994] have shown the impact of no-slip conditions at a fracture's surface on the fracture-matrix exchange; yet we are not aware of analytical attempts to quantify this effect.

[42] Such two-dimensional solutions will enhance the reliability of parametric identification procedures. They can also be incorporated into hybrid (fracture-/continuum-scale or pore-/continuum-scale) models of transport in fractured rock and porous media [*Tartakovsky et al.*, 2008; *Battiato et al.*, 2011], especially those dealing with complex fracture networks.

Appendix A: Green's Functions and Solute Concentrations

A1. Green's Function for Fracture BVP

[43] Two-dimensional Green's function $G^f(x,z;x',z';t-t')$ for the fracture BVP (1), (3a), (3c), and $D_T^f \partial c_f/\partial z(x,z=b,t)=r$ is obtained [*Carslaw and Jaeger*, 1959] as the product of two one-dimensional Green's functions, $G^f = G_x^f G_z^f$, where $G_x^f(x;x';t-t')$ and $G_z^f(z;z';t-t')$ are given by

$$G_x^f = \frac{e^{\frac{u[2(x-x')-u(t-t')]}{4D_L^f}}}{2\sqrt{D_L^f \pi (t-t')}}\left[e^{-\frac{(x-x')^2}{4D_L^f(t-t')}} - e^{-\frac{(x+x')^2}{4D_L^f(t-t')}}\right] \tag{A1}$$

and

$$G_z^f = \frac{1}{b} + \frac{2}{b}\sum_{n=1}^{\infty} e^{-D_T^f \alpha_n^2 (t-t')}\cos(\alpha_n z)\cos(\alpha_n z') \tag{A2}$$

with $\alpha_n = n\pi/b$.

[44] The Laplace transform of G^f has the form

$$\overline{G}^f = \frac{\overline{G}_x^f}{b} + \frac{2}{b}\sum_{n=1}^{+\infty}\cos(\alpha_n z)\cos(\alpha_n z')(s + D_T^f \alpha_n^2)\overline{G}_x^f, \tag{A3}$$

where

$$\overline{G}_x^f = e^{\frac{u(x-x')}{2D_L^f}}\frac{e^{-|x-x'|\gamma} - e^{-(x+x')\gamma}}{\sqrt{u^2 + 4D_L^f s}} \tag{A4}$$

and

$$\gamma = \sqrt{\frac{1}{D_L^f}\left(\frac{u^2}{4D_L^f} + s\right)}. \tag{A5}$$

A2. Green's Function for Matrix BVP

[45] Two-dimensional Green's function $G^m(x,z;x',z';t-t')$ for the matrix BVP (2), (3a), (3d), and $\phi_m D_T^m \partial c_m/\partial z(x,z=b,t)=r$ is expressed as the product of the one-dimensional Green's function $G_x^m(x;x';t-t')$ and $G_z^m(z;z';t-t')$, which are given by [*Carslaw and Jaeger*, 1959]

$$G_x^m = \frac{1}{2\sqrt{\pi D_L^m (t-t')}}\left[e^{-\frac{(x-x')^2}{4D_L^m(t-t')}} - e^{-\frac{(x+x')^2}{4D_L^m(t-t')}}\right] \tag{A6}$$

and

$$G_z^m = \frac{1}{2\sqrt{\pi D_T^m (t-t')}}\left[e^{-\frac{(z-z')^2}{4D_T^m(t-t')}} + e^{-\frac{(z+z'-2b)^2}{4D_T^m(t-t')}}\right]. \tag{A7}$$

[46] The Laplace transform of G^m is

$$\overline{G}^m(s) = \frac{K_0(\gamma_{11}) + K_0(\gamma_{12}) - K_0(\gamma_{21}) - K_0(\gamma_{22})}{2\pi\sqrt{D_L^m D_T^m}}, \tag{A8}$$

where $\gamma_{ij} = \sqrt{(a_i + b_j)s}$ for $i,j = 1,2$, $a_1 = (x-x')^2/D_L^m$, $a_2 = (x+x')^2/D_L^m$, $b_1 = (z-z')^2/D_T^m$, and $b_2 = (z+z'-2b)^2/D_T^m$.

A3. Concentrations in Fracture and Matrix

[47] Solutions of the fracture and matrix BVPs, expressed in terms of the corresponding Green's functions G^f and G^m, can be written as

$$\begin{aligned} c_f(x,z,t) = {} & \int_0^b\int_0^\infty c_f^0(x',z')G^f(\cdot;\cdot;t)\mathrm{d}x'\mathrm{d}z' \\ & + \int_0^t\int_0^b c_0(z',t')\left[uG^f + D_L^f\frac{\partial G^f}{\partial x'}\right](\cdot;0,z';\cdot)\mathrm{d}z'\mathrm{d}t' \\ & + \int_0^t\int_0^\infty r(x',t')G^f(\cdot;x',b;\cdot)\mathrm{d}x'\mathrm{d}t' \\ & + \int_0^t\int_0^b\int_0^\infty f(x',z',t')G^f(\cdot;\cdot;\cdot)\mathrm{d}x'\mathrm{d}z'\mathrm{d}t' \end{aligned} \tag{A9}$$

and

$$\begin{aligned} c_m(x,z,t) = {} & \int_0^\infty\int_0^\infty c_m^0(x',z')G^m(\cdot;\cdot;t)\mathrm{d}x'\mathrm{d}z' \\ & - \frac{1}{\phi_m}\int_0^t\int_0^\infty r(x',t')G^m(\cdot;x',b;\cdot)\mathrm{d}x'\mathrm{d}t'. \end{aligned} \tag{A10}$$

Appendix B: Solution of Fredholm Equation

[48] To facilitate the solution of the Fredholm equation of the first kind (16), we transform its left-hand side into

$$\int_0^\infty \mathcal{I}(x')\mathrm{d}x' = \int_0^1\left[\mathcal{I}(x') + \mathcal{I}\left(\frac{1}{x'}\right)\frac{1}{x'^2}\right]\mathrm{d}x', \tag{B1}$$

where $\mathcal{I}(x') \equiv \mathcal{K}(x,x',s)\overline{R}(x',s)$. The integration interval is subdivided into N_x subintervals of length $\Delta x = 1/N_x$, so that

$$\int_0^\infty \mathcal{I}(x')\mathrm{d}x' = \sum_{j=0}^{N_x}\int_{x_j}^{x_{j+1}}\left[\mathcal{I}(x') + \mathcal{I}\left(\frac{1}{x'}\right)\frac{1}{x'^2}\right]\mathrm{d}x' \tag{B2}$$

with $x_j = j\Delta x$. The change of the integration variable $x = 1/x'$ in the second term of the integrand yields

$$\int_0^{\infty} \mathcal{I}(x')\mathrm{d}x' = \sum_{j=0}^{N_x} \left[\int_{x_j}^{x_{j+1}} \mathcal{I}(x')\mathrm{d}x' + \int_{1/x_{j+1}}^{1/x_j} \mathcal{I}(x')\mathrm{d}x' \right]. \quad \text{(B3)}$$

Thus, the integral in (16) is transformed into a sum of $N_\chi = 2N_x$ integrals

$$\int_0^{\infty} \mathcal{I}(x')\mathrm{d}x' = \sum_{j=0}^{N_\chi} \int_{\chi_j}^{\chi_{j+1}} \mathcal{I}(x')\mathrm{d}x', \quad \text{(B4)}$$

where $\chi_j = j\Delta x$ for $j = 0, \ldots, N_x$ and $\chi_j = 1/(j\Delta x)$ for $j = N_x, \ldots, 2N_x$.

[49] The expected behavior of $\overline{R}(x', s)$ on the integration intervals $[\chi_j, \chi_{j+1}]$ determines the numerical approximation of the corresponding integrals of $\mathcal{I}(x') \equiv \mathcal{K}(x, x', s)\overline{R}(x', s)$ [*Fogden et al.*, 1988]. If $\overline{R}(x, s)$ varies slowly with $x \in [\chi_j, \chi_{j+1}]$, then

$$\int_{\chi_j}^{\chi_{j+1}} \mathcal{I}(x')\mathrm{d}x' \approx \overline{R}(\breve{x}_j) \int_{\chi_j}^{\chi_{j+1}} \breve{\mathcal{K}}(x, x', s)\mathrm{d}x'. \quad \text{(B5a)}$$

If $\overline{R}(x, s)$ varies quickly with $x \in [\chi_j, \chi_{j+1}]$, then

$$\int_{\chi_j}^{\chi_{j+1}} \mathcal{I}(x')\mathrm{d}x' \approx \breve{R}(\breve{x}_j) \int_{\chi_j}^{\chi_{j+1}} \breve{\mathcal{K}}(x, x', s)\mathrm{d}x'. \quad \text{(B5b)}$$

In (B5a) and (B5b), $\breve{x}_j = (\chi_j + \chi_{j+1})/2$, $\breve{\mathcal{K}}(x, x', s) = \breve{\mathcal{K}}(x, x', s)/x'$, and $\breve{R}(\breve{x}_j, s) = \breve{x}_j \overline{R}(\breve{x}_j, s)$.

[50] This approximation enables us to replace the Fredholm equation (16) with one of the two linear systems of algebraic equations,

$$\mathbf{A}\mathbf{r} = \mathbf{b} \quad \text{or} \quad \breve{\mathbf{A}}\,\breve{\mathbf{r}} = \mathbf{b}, \quad \text{(B6)}$$

depending on whether $\overline{R}(x, s)$ varies slowly or quickly with x. The $N_\chi \times N_\chi$ matrices $\mathbf{A}$ and $\breve{\mathbf{A}}$ have components

$$A_{ij} = \int_{\chi_j}^{\chi_{j+1}} \mathcal{K}(x_i, x')\mathrm{d}x', \qquad \breve{A}_{ij} = \int_{\chi_j}^{\chi_{j+1}} \mathcal{K}\frac{\mathrm{d}x'}{x'}, \quad \text{(B7)}$$

and the components of N_χ-dimensional vectors $\mathbf{r}$, $\breve{\mathbf{r}}$, and $\mathbf{b}$ are given by

$$r_j = \overline{R}(\breve{x}_j, s), \qquad \breve{r}_j = \breve{x}_j \overline{R}(\breve{x}_j, s), \quad \text{(B8)}$$

$$b_j = -\sqrt{D_L^f D_T^f} F_1^*(x_j, s). \quad \text{(B9)}$$

The matrix components $\breve{A}_{ij}$ are computed numerically, while the components A_{ij} are evaluated analytically as follows.

[51] Substituting (17) into the first relation in (B7) yields

$$\begin{aligned} A_{ij} = {} & \frac{1}{2} H_f^*(x_{fi}, \chi_j, \chi_{j+1}, s_f) \\ & + \sum_{n=1}^{\infty} H_f^*(x_{fi}, \chi_j, \chi_{j+1}, s_f + D_T^f \alpha_n^2) \\ & + D_{fm} H_m^*(x_{mi}, \chi_j, \chi_{j+1}, s_m), \end{aligned} \quad \text{(B10)}$$

where

$$\begin{aligned} H_f^*(x_f, \chi_j, \chi_{j+1}, s_f) &= \int_{\chi_j}^{\chi_{j+1}} F_2^*(x_f, x_f', s_f)\mathrm{d}x_f' \\ &= \frac{h_f(x, \chi_j, \chi_{j+1}, s)}{\sqrt{Pe^2/4 + s_f}} \end{aligned} \quad \text{(B11)}$$

and

$$\begin{aligned} H_m^*(x_{mi}, \chi_j, \chi_{j+1}, s_m) &= \int_{\chi_j}^{\chi_{j+1}} F_3^*(x_m, x_m', b, s_m)\mathrm{d}x_m' \\ &= \mathcal{T}_1(k, x, x') - \mathcal{T}_2(k, x, x'). \end{aligned} \quad \text{(B12)}$$

[52] In (B11),

$$\begin{aligned} h_f = {} & \frac{e^{(c-\gamma_1 a)(x-\chi_j)} - 1}{c - \gamma_1 a} - \frac{e^{(c-\gamma_2 a)(x-\chi_{j+1})} - 1}{c - \gamma_2 a} \\ & + \frac{e^{x(c-a)-\chi_{j+1}(c+a)}}{c + a} - \frac{e^{x(c-a)-\chi_j(c+a)}}{c + a}, \end{aligned} \quad \text{(B13)}$$

where $a^2 = [u^2/(4D_L^f) + s]/D_L^f$, $c = u/(2D_L^f)$, $\gamma_1 = \mathrm{sign}(x - \chi_j)$, and $\gamma_2 = \mathrm{sign}(x - \chi_{j+1})$.

[53] In (B12),

$$\begin{aligned} \mathcal{T}_1 = {} & \frac{\pi}{2}(x + x') \left\{ L_{-1}\left[\sqrt{k(x + x')^2}\right] K_0\left[\sqrt{k(x + x')^2}\right] \right. \\ & \left. + L_0\left[\sqrt{k(x + x')^2}\right] K_1\left[\sqrt{k(x + x')^2}\right] \right\} \end{aligned} \quad \text{(B14)}$$

and

$$\begin{aligned} \mathcal{T}_2 = {} & \frac{\pi}{2}(x - x') \left\{ L_{-1}\left[\sqrt{k(x - x')^2}\right] K_0\left[\sqrt{k(x - x')^2}\right] \right. \\ & \left. + L_0\left[\sqrt{k(x - x')^2}\right] K_1\left[\sqrt{k(x - x')^2}\right] \right\}, \end{aligned} \quad \text{(B15)}$$

where $k = s/D_L^m$ and $L_n(\cdot)$ denotes the modified Struve function of order n.

[54] **Acknowledgments.** This research was supported by the Office of Science of the U.S. Department of Energy (DOE) under the Scientific Discovery through Advanced Computing (SciDAC) program and by the French National Research Agency ANR through the MICAS project (ANR-07-CIS7-004).

References

Altmann, S., C. Tournassat, F. Goutelard, J.-C. Parneix, T. Gimmi, and N. Maes (2012), Diffusion-driven transport in clayrock formations, *Appl. Geochem.*, *27*, 463–478, doi:10.1016/j.apgeochem.2011.09.015.

Battiato, I., and D. M. Tartakovsky (2011), Applicability regimes for macroscopic models of reactive transport in porous media, *J. Contam. Hydrol.*, *120–121*, 18–26, doi:10.1016/j.jconhyd.2010.05.005.

Battiato, I., D. M. Tartakovsky, A. M. Tartakovsky, and T. Scheibe (2009), On breakdown of macroscopic models of mixing-controlled heterogeneous reactions in porous media, *Adv. Water Resour.*, *32*, 1664–1673, doi:10.1016/j.advwatres.2009.08.008.

Battiato, I., D. M. Tartakovsky, A. M. Tartakovsky, and T. D. Scheibe (2011), Hybrid models of reactive transport in porous and fractured media, *Adv. Water Resour.*, *34*(9), 1140–1150, doi:10.1016/j.advwatres.2011.01.012.

Bodin, J., F. Delay, and G. de Marsily (2003), Solute transport in a single fracture with negligible matrix permeability: 1. Fundamental mechanisms, *Hydrogeol. J.*, *11*(4), 418–433.

Buckley, R. L., and S. K. Loyalka (1994), Numerical-stidies of solute transport in a fracture surrounded by a rock matrix–effect of lateral diffusion and chemical-reaction on the overall dispersion, *Ann. Nucl. Energy*, *21*(8), 461–494.

Callahan, T. J., P. W. Reimus, R. S. Bowman, and M. J. Haga (2000), Using multiple experimental methods to determine fracture/matrix interactions and dispersion of nonreactive solutes in saturated volcanic tuff, *Water Resour. Res.*, *36*(12), 3547–3558.

Carslaw, H. S., and J. C. Jaeger (1959), *Conduction of Heat in Solids*, 520 pp., Oxford Univ. Press, New York.

Fogden, A., K. A. Landman, and L. R. White (1988), Contaminant transport in fractured porous media: Steady state solutions by a boundary integral method, *Water Resour. Res.*, *24*(8), 1384–1396.

Liu, H. H., Y. Q. Zhang, and F. J. Molz (2007), Scale dependence of the effective matrix diffusion coefficient: Some analytical results, *Vadose Zone J.*, *6*(3), 679–683.

Maloszewski, P., and A. Zuber (1993), Tracer experiments in fractured rocks: Matrix diffusion and the validity of models, *Water Resour. Res.*, *29*(8), 2723–2735.

Moreno, L., I. Neretnieks, and T. Eriksen (1985), Analysis of some laboratory tracer runs in natural fissures, *Water Resour. Res.*, *21*(7), 951–958.

Roubinet, D., H.-H. Liu, and J. R. de Dreuzy (2010), A new particle-tracking approach to simulating transport in heterogeneous fractured porous media, *Water Resour. Res.*, *46*, W11507, doi:10.1029/2010WR009371.

Sudicky, E. A., and E. O. Frind (1982), Contaminant transport in fractured porous media: Analytical solutions for a system of parallel fractures, *Water Resour. Res.*, *18*(6), 1634–1642.

Tang, D. H., E. O. Frind, and E. A. Sudicky (1981), Contaminant transport in fractured porous media: Analytical solution for a single fracture, *Water Resour. Res.*, *17*(3), 555–564.

Tartakovsky, A. M., D. M. Tartakovsky, T. D. Scheibe, and P. Meakin (2008), Hybrid simulations of reaction-diffusion systems in porous media, *SIAM J. Sci. Comput.*, *30*(6), 2799–2816.

Van Loon, L. R., J. M. Soler, W. Müller, and M. H. Bradbury (2004), Anisotropic diffusion in layered argillaceous rocks: A case study with Opalinus Clay, *Environ. Sci. Technol.*, *38*(21), 5721–5728.

Zhan, H. B., Z. Wen, G. H. Huang, and D. Sun (2009), Analytical solution of two-dimensional solute transport in an aquifer-aquitard system, *J. Contam. Hydrol.*, *107*(3–4), 162–174.

Zhou, Q. L., H. H. Liu, F. J. Molz, Y. Q. Zhang, and G. S. Bodvarsson (2007), Field-scale effective matrix diffusion coefficient for fractured rock: Results from literature survey, *J. Contam. Hydrol.*, *93*(1–4), 161–187.

J.-R. de Dreuzy, Géosciences Rennes, UMR CNRS 6118, Université de Rennes I, Campus de Beaulieu, F-35042 Rennes CEDEX, France.

D. Roubinet and D. M. Tartakovsky, Department of Mechanical and Aerospace Engineering, University of California, San Diego, 9500 Gilman Dr., La Jolla, CA 92093, USA. (dmt@ucsd.edu)